Article

Spectroscopic and Computational Studies of the ATP:Corrinoid Adenosyltransferase (CobA) from *Salmonella enterica*: Insights into the Mechanism of Adenosylcobalamin Biosynthesis

Troy A. Stich, Nicole R. Buan, Jorge C. Escalante-Semerena, and Thomas C. Brunold

J. Am. Chem. Soc., **2005**, 127 (24), 8710-8719• DOI: 10.1021/ja042142p • Publication Date (Web): 26 May 2005

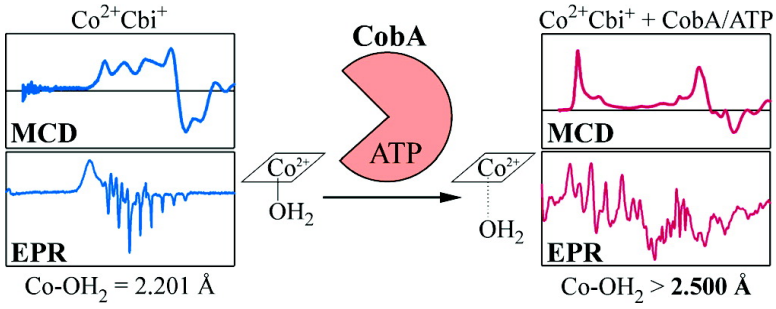

More About This Article

Additional resources and features associated with this article are available within the HTML version:

- Supporting Information
- Links to the 7 articles that cite this article, as of the time of this article download
- Access to high resolution figures
- Links to articles and content related to this article
- Copyright permission to reproduce figures and/or text from this article

View the Full Text HTML

J|A|C|S
ARTICLES
Published on Web 05/26/2005

Spectroscopic and Computational Studies of the ATP:Corrinoid Adenosyltransferase (CobA) from *Salmonella enterica*: Insights into the Mechanism of Adenosylcobalamin Biosynthesis

Troy A. Stich,[†] Nicole R. Buan,[‡] Jorge C. Escalante-Semerena,[‡] and Thomas C. Brunold*,[†]

Contribution from the Departments of Chemistry and Bacteriology, University of Wisconsin—Madison, Madison, Wisconsin 53706

Received December 31, 2004; E-mail: brunold@chem.wisc.edu

Abstract: CobA from *Salmonella enterica* is a member of an enzymatic system responsible for the de novo biosynthesis of adenosylcobalamin (AdoCbl), catalyzing the formation of the essential Co−C bond by transferring the adenosyl group from a molecule of ATP to a transient Co^{1+}corrinoid species generated in the enzyme active site. A particularly fascinating aspect of this reaction is that the flavodoxin in vivo reducing agent that serves as the electron donor to CobA possesses a reduction potential that is considerably more positive than that of the $Co^{2+/1+}$ couple of the corrinoid substrate. To explore how CobA may overcome this challenge, we have employed electronic absorption, magnetic circular dichroism, and electron paramagnetic resonance (EPR) spectroscopies to probe the interaction between Co^{3+}- and Co^{2+}corrinoids and the enzyme active site. Our data reveal that while Co^{3+}corrinoids interact only weakly with CobA, Co^{2+}corrinoids undergo partial conversion to a new paramagnetic species that can be obtained in nearly quantitative yield when CobA is preincubated with the co-substrate ATP. This "activated" species is characterized by a distinct set of ligand field transitions in the near-IR spectral region and EPR parameters that are unprecedented for Co^{2+}corrinoids. Analysis of these data on the basis of qualitative spectral correlations and density functional theory computations reveals that this unique Co^{2+}corrinoid species possesses an essentially square-planar Co^{2+} center that lacks any significant axial bonding interactions. Possible implications of these findings for the mechanism of $Co^{2+} \rightarrow Co^{1+}$ reduction employed by CobA and Co−C bond-forming enzymes in general are explored.

1. Introduction

Vitamin B_{12} (cyanocobalamin, CNCbl) is a nutrient necessary to sustain life in all animals, including humans; yet, only a few species of prokaryotes (including *Salmonella enterica*) are able to accomplish the de novo synthesis of this complex cofactor.[1] In CNCbl, the four pyrrolic nitrogen atoms of a highly substituted macrocycle, termed the corrin ring, equatorially ligate a low-spin Co^{3+} ion (Figure 1).[2] The "lower" axial face of the Co is coordinated by a nitrogen atom from a 5,6-dimethylbenzimidazole (DMB) base, which is part of the nucleotide terminus of a molecular loop tethered to the corrin ring at C^{17}. A variety of ligands can bind in the "upper" axial position (e.g., CN^- as in CNCbl); however, cobalamin is biologically active only when this position is occupied by a methyl group, as in methylcobalamin (MeCbl), or an adenosyl group, as in coenzyme B_{12} (adenosylcobalamin, AdoCbl).[3]

While higher order organisms lack the complete biosynthetic machinery needed to manufacture AdoCbl de novo, they possess adenosyltransferases that are able to catalyze the replacement of the upper axial ligand of exogenous cobalamins with the 5′-deoxyadenosyl (Ado) group derived from a molecule of ATP.[4,5] The Ado group is bound to the Co center through the 5′-C, yielding one of Nature's few examples of a stable organometallic bond.[6] In humans, AdoCbl is employed as the cofactor for methylmalonyl-CoA mutase (MMCM), the isomerase responsible for catalyzing the rearrangement of the catabolite methylmalonyl-CoA to succinyl-CoA.[7] Malfunction of the human adenosyltransferase (hATR) can lead to potentially fatal disorders, such as methylmalonic aciduria and metabolic ketoacidosis.[8]

The biosynthetic route that leads to corrin-based cofactors utilizes over 25 enzymes to convert 5-aminolaevulinic acid to

[†] Department of Chemistry.
[‡] Department of Bacteriology.

(1) Warren, M. J.; Raux, E.; Schubert, H. L.; Escalante-Semerena, J. C. *Nat. Prod. Rep.* **2002**, *19*, 390−412.
(2) Randaccio, L.; Furlan, M.; Geremia, S.; Slouf, M.; Srnova, I.; Toffoli, D. *Inorg. Chem.* **2000**, *39*, 3403−3413.
(3) Banerjee, R.; Ragsdale, S. W. *Annu. Rev. Biochem.* **2003**, *72*, 209−247.
(4) Escalante-Semerena, J. C.; Suh, S. J.; Roth, J. R. *J. Bacteriol.* **1990**, *172*, 273−280.
(5) Fenton, W. A.; Rosenberg, L. E. *Biochem. Biophys. Res. Commun.* **1981**, *98*, 283−289.
(6) Ouyang, L. Z.; Rulis, P.; Ching, W. Y.; Nardin, G.; Randaccio, L. *Inorg. Chem.* **2004**, *43*, 1235−1241.
(7) Banerjee, R. *Biochemistry* **2001**, *40*, 6191−6198.

10.1021/ja042142p CCC: $30.25

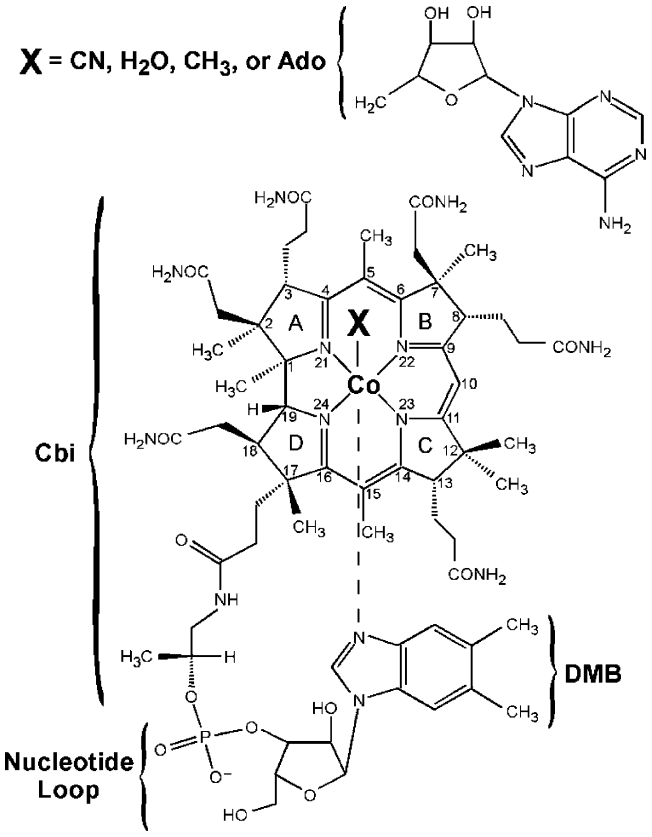

Figure 1. Chemical structure and numbering scheme for Co^{3+}cobalamins. Note that Co^{3+}cobinamides lack the nucleotide loop and DMB moiety and instead bind an H_2O molecule in the lower axial position.

cobyrinic acid, a cobalamin precursor that possesses all of the necessary functionality save the nucleotide loop and the Ado upper axial ligand. Cobyrinic acid is then adenosylated by a 21 kDa homodimeric adenosyltransferase (CobA) before entering the nucleotide loop assembly pathway.[9,10] In addition to CobA, *S. enterica* employs two other evolutionarily distinct adenosyltransferases, PduO and EutT,[11,12] yet CobA is the only transferase that efficiently adenosylates exogenous cobalamins as well as incomplete corrinoids (such as cobinamides, Figure 1) that lack part or all of the nucleotide loop. Additionally, CobA is responsible for maintaining a basal concentration of AdoCbl to promote transcription of the *eut* operon that encodes proteins needed for the catabolism of ethanolamine.[12,13] Included among the *eut* proteins is EutT, a presumably Fe−S cluster-containing adenosyltransferase[12] that provides a ready supply of adenosylated cobalamin to the *eutBC* gene product, an AdoCbl-dependent ethanolamine ammonia lyase (EAL).[14] PduO fulfills a similar role for the cobalamin-dependent degradation of 1,2-propanediol by the enzyme diol dehydratase (DD).[11] Interestingly, PduO from *S. enterica* bears significant sequence homology (26% sequence identity) to hATR that is co-translated with MMCM.[15,16]

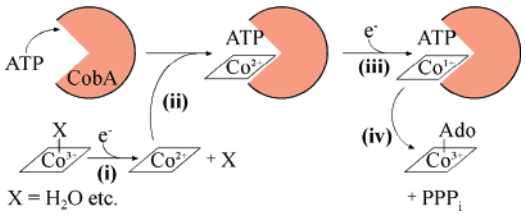

Figure 2. Proposed reaction mechanism for the adenosylation of corrinoids catalyzed by CobA (adapted from ref 22). The cobalt-containing corrinoid is reduced to the Co^{2+} oxidation state (step i) by the reducing environment of the cytoplasm. Upon formation of the ternary complex (step ii), a flavin mononucleotide (FMN)-dependent reductase, FldA, supplies the second electron needed to generate the strongly nucleophilic Co^{1+}corrinoid (step iii) that then attacks the 5′-carbon of ATP to form the Co−C bond (step iv).

Its ability to adenosylate both scavenged cobalamins and incomplete corrinoids originating from the de novo assembly pathway makes CobA an ideal target for studying the generic mechanistic requirements for adenosyl-group transfer. The current proposal for the CobA reaction mechanism is depicted in Figure 2. While the general mechanism of the adenosyl-group transfer is fairly well established, several important questions concerning specific events in this process remain unanswered. Perhaps the most interesting aspect of the mechanism depicted in Figure 2 (from the point of view of electronic structure) is that CobA is capable of generating a transient Co^{1+}corrinoid intermediate even though the $Co^{2+/1+}$ reduction midpoint potential of unbound Co^{2+}Cbl ($E° = -610$ mV)[17] is well below that of the semiquinone/reduced flavin couple of FldA ($E° = -440$ mV).[18] Thus, an understanding of the mechanism by which CobA catalyzes Co−C bond formation provides a suitable framework not only for the subsequent investigation of the other adenosyltransferases described above but also for studies of MeCbl-dependent enzymes, such as methionine synthase (MetH) and the corrinoid Fe−S protein (CFeSP), in which formation of a Co^{1+}Cbl intermediate constitutes one of the key steps in their respective reactivation mechanisms.[3]

Previously, our group has characterized the electronic structures of free cobalamins and cobinamides in both their Co^{3+} and Co^{2+} oxidation states using an array of spectroscopic methods in conjunction with density functional theory (DFT) calculations.[19,20] Using our insights gained in these studies as a foundation, we have begun to examine the nature of enzyme-induced activation of corrinoids for several representative cobalamin-dependent systems, including MMCM,[21] MetH, glutamate mutase (GM), and CFeSP. This report summarizes our efforts to characterize spectroscopically substrate binding events and intermediates involved in the adenosylation pathway

(8) Dobson, C. M.; Wai, T.; Leclerc, D.; Kadir, H.; Narang, M.; Lerner-Ellis, J. P.; Hudson, T. J.; Rosenblatt, D. S.; Gravel, R. A. *Hum. Mol. Genet.* **2002**, *11*, 3361−3369.
(9) Bauer, C. B.; Fonseca, M. V.; Holden, H. M.; Thoden, J. B.; Thompson, T. B.; Escalante-Semerena, J. C.; Rayment, I. *Biochemistry* **2001**, *40*, 361−374.
(10) Maggio-Hall, L. A.; Escalante-Semerena, J. C. *Proc. Natl. Acad. Sci. U.S.A.* **1999**, *96*, 11798−11803.
(11) Johnson, C. L. V.; Pechonick, E.; Park, S. D.; Havemann, G. D.; Leal, N. A.; Bobik, T. A. *J. Bacteriol.* **2001**, *183*, 1577−1584.
(12) Buan, N. R.; Suh, S. J.; Escalante-Semerena, J. C. *J. Bacteriol.* **2004**, *186*, 5708−5714.
(13) Sheppard, D. E.; Penrod, J. T.; Bobik, T.; Kofoid, E.; Roth, J. R. *J. Bacteriol.* **2004**, *186*, 7635−7644.
(14) Kofoid, E.; Rappleye, C.; Stojiljkovic, I.; Roth, J. *J. Bacteriol.* **1999**, *181*, 5317−5329.
(15) Dobson, C. M.; Wai, T.; Leclerc, D.; Wilson, A.; Wu, X. C.; Dore, C.; Hudson, T.; Rosenblatt, D. S.; Gravel, R. A. *Proc. Natl. Acad. Sci. U.S.A.* **2002**, *99*, 15554−15559.
(16) Leal, N. A.; Park, S. D.; Kima, P. E.; Bobik, T. A. *J. Biol. Chem.* **2003**, *278*, 9227−9234.
(17) Lexa, D.; Saveant, J.-M. *Acc. Chem. Res.* **1983**, *16*, 235−243.
(18) Hoover, D. M.; Jarrett, J. T.; Sands, R. H.; Dunham, W. R.; Ludwig, M. L.; Matthews, R. G. *Biochemistry* **1997**, *36*, 127−138.
(19) Stich, T. A.; Brooks, A. J.; Buan, N. R.; Brunold, T. C. *J. Am. Chem. Soc.* **2003**, *125*, 5897−5914.
(20) Stich, T. A.; Buan, N. R.; Brunold, T. C. *J. Am. Chem. Soc.* **2004**, *126*, 9735−9749.
(21) Brooks, A. J.; Vlasie, M.; Banerjee, R.; Brunold, T. C. *J. Am. Chem. Soc.* **2004**, *126*, 8167−8180.

employed by CobA. Specifically, MCD spectroscopy has been used to probe changes in the Co^{2+} ligand field (LF, d→d) transition energies upon binding of Co^{2+}Cbl and Co^{2+}-cobinamide ($Co^{2+}Cbi^{+}$, Figure 1) to the CobA active site. These data have been interpreted within the framework of spectral correlations to free Co^{3+}- and Co^{2+}corrinoids as well as DFT calculations on cofactor models and cobalamin analogues. Collectively, our results provide detailed insight into the mechanism by which CobA tunes the $Co^{2+/1+}$ reduction potential so as to enable the formation of an active-site bound Co^{1+}-corrinoid "supernucleophile" that is the key reactive intermediate in the adenosylation pathway.

2. Experimental Section

Cofactors and Chemicals. Aquacobalamin (H_2OCbl^{+}), dicyanocobinamide ($(CN)_2Cbi$), AdoCbl, and sodium borohydride ($NaBH_4$) were purchased from Sigma and used as obtained. Diaquacobinamide ($(H_2O)_2Cbi^{2+}$) was prepared by reducing a solution of $(CN)_2Cbi$ with BH_4^{-}, loading the reaction mixture onto a C_{18} SepPack column, and quenching with doubly distilled H_2O. The $(H_2O)_2Cbi^{2+}$ product was eluted with methanol and characterized by mass spectrometry and Abs spectroscopy. Co^{2+}Cbl and $Co^{2+}Cbi^{+}$ were prepared anaerobically by BH_4^{-} reduction of H_2OCbl^{+} and $(H_2O)_2Cbi^{2+}$, respectively.

Purification of CobA Enzyme. The ATP:corrinoid adenosyltransferase CobA from *Salmonella enterica* was overexpressed and isolated using previously published procedures.[22] CobA purity (>95% homogeneity) was monitored with SDS−PAGE, and enzymatic activity (19.74 nmol of AdoCbl produced/min·mg of CobA) was determined using the corrinoid adenosylation assay developed previously.[22] All samples used in this study contained 0.40 mM CobA in 50 mM TRIS−HCl buffer (pH 8.0), 0.5 mM dithiothreitol (DTT) to enhance protein stability, and 60% (v/v) of the glassing agent glycerol.

Sample Preparation. Solutions of the free corrinoids and CobA were purged separately with N_2 gas for 20 min at 4 °C and subsequently combined in a 0.9:1.0 ratio in a sealed anaerobic vial. The resulting mixtures were equilibrated for 5 min under constant N_2 pressure and then injected simultaneously into MCD cells and quartz EPR tubes that were then immediately frozen in liquid N_2. CobA samples containing the co-substrate ATP were prepared by anaerobically incubating the enzyme for 20 min at 4 °C with a 20-fold molar excess of ATP.

Spectroscopy. Low-temperature electronic Abs, CD, and MCD spectra were acquired using a Jasco J-715 spectropolarimeter in conjunction with an Oxford Instruments SpectroMag-4000 8T magnetocryostat. All MCD spectra shown in this paper were obtained by taking the difference between the spectra collected with the magnetic field aligned parallel and antiparallel to the light propagation axis. X-band EPR data were collected using a Bruker ESP 300E spectrometer equipped with an Oxford ESR 900 continuous flow liquid helium cryostat, an Oxford ITC4 temperature controller, and a Varian EIP model 625A CW frequency counter. All spectra were accumulated under nonsaturating conditions (see caption of Figure 6 for details of spectral acquisition). EPR data were simulated using the WEPR program written by Dr. Frank Neese.[23] Complete parameter sets employed for the EPR simulations are given in the Supporting Information.

Computations. (i) Models. A computational model of $Co^{2+}Cbi^{+}$ ("unperturbed" model) was generated starting from the published crystal structure coordinates of Co^{2+}Cbl,[24] replacing the lower axial ligand by an H_2O molecule and truncating the peripheral corrin ring substituents, as described in our earlier work on free Co^{2+}corrinoids.[20] To generate

Scheme 1. Chemical Structure of $[Co(Me_6[14]dieneN_4)]$

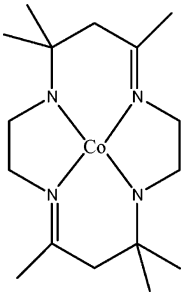

$Co^{2+}Cbi^{+}$ models along the lower ligand dissociation pathway, the Co−OH_2 bond was systematically lengthened in increments of 0.05 Å from the unperturbed distance of 2.201 Å, while the coordinates of all other atoms were kept fixed.

For computational studies on *N-rac*-[Co^{2+}-5,7,7,12,14,14-hexamethyl-1,4,8,11-tetraazacyclotetradeca-4,11-diene(H_2O)] (abbreviated $[Co(Me_6[14]dieneN_4)(H_2O)]$, Scheme 1), the input geometry was based on the corresponding X-ray crystal structure coordinates,[25] where the $Me_6[14]dieneN_4$ ligand H atoms were added at a distance of 1.1 Å from their respective C atoms. The coordinates of the H atoms of the axially bound water molecule were energy minimized using the Amsterdam Density Functional (ADF) 2003.02 suite of programs[26−28] with the Vosko−Wilk−Nusair local density approximation (VWN)[29] and the gradient corrections of Becke[30] and Perdew[31] for exchange and correlation, respectively. This calculation was carried out on an Intel Xeon cluster (ACE computers) employing ADF basis set IV and an integration constant of 4.0. Atomic coordinates for the $Co^{2+}Cbi^{+}$ and $[Co(Me_6[14]dieneN_4)(H_2O)]$ models are provided in the Supporting Information.

(ii) Single Point DFT Calculations. Ground state DFT calculations were executed on a desktop PC using the ORCA 2.2 software package developed by Dr. Frank Neese (MPI Mülheim, Germany).[32] The Perdew−Wang LDA (PW-LDA)[33] in conjunction with the gradient corrections by Becke[34] and Perdew[31] was chosen for all DFT computations, following our earlier work on free Co^{2+}corrinoids. Electronic excitation energies and intensities for all models were calculated by the TD-DFT method[35−37] within the Tamm−Dancoff approximation[38,39] as implemented in ORCA 2.2. The predicted Abs spectra were simulated assuming that each electronic transition gives rise to a Gaussian band with full width at half-maximum of $\nu_{1/2} = 1250\ cm^{-1}$. Finally, molecular *g* values and hyperfine parameters were calculated with the ORCA program by solving the coupled-perturbed SCF (CP-SCF) equations[40] employing the PW-LDA functional. Additional details (e.g., basis set descriptions) are provided in the Supporting Information.

(22) Suh, S.-J.; Escalante-Semerena, J. C. *J. Bacteriol.* **1995**, *177*, 921−925.
(23) Neese, F. *Electronic Structure and Spectroscopy of Novel Copper Chromophores in Biology*. Ph.D. Thesis, University of Konztanz, 1997.
(24) Kräutler, B.; Keller, W.; Kratky, C. *J. Am. Chem. Soc.* **1989**, *111*, 8936−8938.
(25) Szalda, D. J.; Schwarz, C. L.; Endicott, J. F.; Fujita, E.; Creutz, C. *Inorg. Chem.* **1989**, *28*, 3214−3219.
(26) te Velde, G.; Bickelhaupt, F. M.; van Gisbergen, S. J. A.; Guerra, C. F.; Baerends, E. J.; Snijders, J. G.; Ziegler, T. *J. Comput. Chem.* **2001**, *22*, 931−967.
(27) Guerra, C. F.; Snijders, J. G.; te Velde, G.; Baerends, E. J. *Theor. Chem. Acc.* **1998**, *99*, 391−403.
(28) *ADF 2003.01*, SCM, Theoretical Chemistry, Vrije Universiteit, Amsterdam, The Netherlands, http://www.scm.com.
(29) Vosko, S. H.; Wilk, L.; Nusair, M. *Can. J. Phys.* **1980**, *58*, 1200−1211.
(30) Becke, A. D. *Phys. Rev. A* **1988**, *38*, 3098−3100.
(31) Perdew, J. P. *Phys. Rev. B* **1986**, *33*, 8822−8824.
(32) Neese, F.; Solomon, E. I. *Inorg. Chem.* **1999**, *38*, 1847−1865.
(33) Perdew, J. P.; Wang, Y. *Phys. Rev. B* **1992**, *45*, 13244−13249.
(34) Becke, A. D. *J. Chem. Phys.* **1986**, *84*, 4524−4529.
(35) Bauernschmitt, R.; Ahlrichs, R. *Chem. Phys. Lett.* **1996**, *256*, 454−464.
(36) Casida, E. M.; Jamorski, C.; Casida, K. C.; Salahub, D. R. *J. Chem. Phys.* **1998**, *108*, 4439−4449.
(37) Stratmann, R. E.; Scuseria, G. E.; Frisch, M. J. *J. Chem. Phys.* **1998**, *109*, 8218−8224.
(38) Hirata, S.; Head-Gordon, M. *Chem. Phys. Lett.* **1999**, *314*, 291−299.
(39) Hirata, S.; Head-Gordon, M. *Chem. Phys. Lett.* **1999**, *302*, 375−382.
(40) Neese, F. *J. Chem. Phys.* **2001**, *115*, 11080−11096.

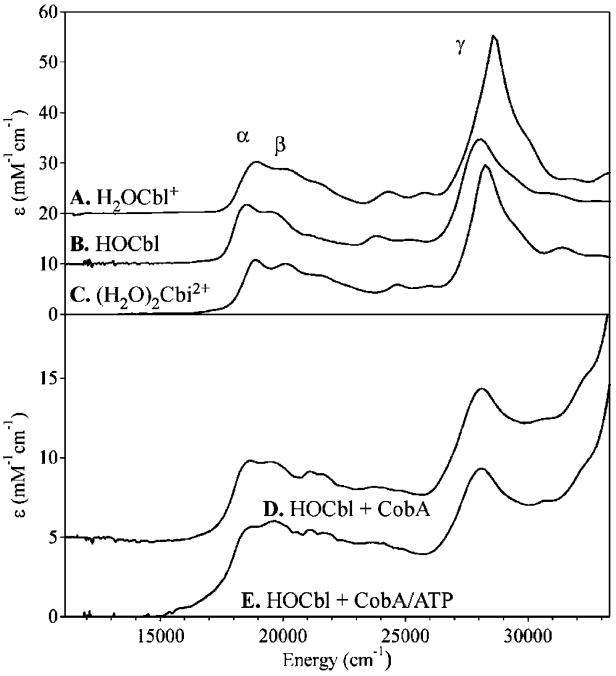

Figure 3. Abs spectra at 4.5 K of (top panel) the free Co^{3+}corrinoids, (A) H_2OCbl^+ (pH 5), (B) HOCbl (pH 9), and (C) $(H_2O)_2Cbl^+$, compared to spectra (bottom panel) of (D) HOCbl in the presence of CobA and (E) HOCbl in the presence of the CobA/ATP complex.

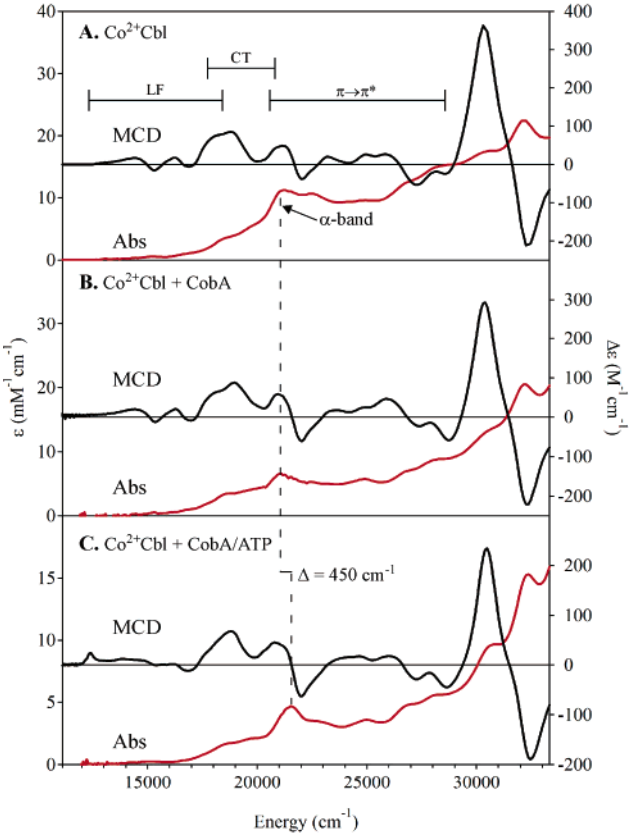

Figure 4. Abs (red traces, left axis) and 7 T MCD (black traces, right axis) spectra recorded at 4.5 K of (A) free $Co^{2+}Cbl$, (B) $Co^{2+}Cbl$ in the presence of CobA, and (C) $Co^{2+}Cbl$ in the presence of the CobA/ATP complex.

3. Results and Analysis.

3.1. Co^{3+}Corrinoid↔CobA Interaction. In our previous Abs and MCD spectroscopic and DFT computational studies of free Co^{3+}corrinoid species,[19] we found that the axial ligand basicity modulates the mixing of Co 3d-orbitals with the corrin ring π/π^* frontier molecular orbitals (MOs), thereby varying the energy of the lowest-energy corrin-based $\pi\rightarrow\pi^*$ (cor $\pi\rightarrow\pi^*$) transition that is responsible for the so-called α-band in the corresponding Abs spectra. Therefore, the position of the α-band provides a sensitive reporter of changes in the axial ligation upon binding of a given Co^{3+}corrinoid to a protein active site. Using this relationship between shifts of the α-band position and axial perturbations, the nature of the interaction between the substrate H_2OCbl^+ and CobA was monitored in both the absence and the presence of the co-substrate ATP.

H_2OCbl^+ + CobA. The Abs spectra of unbound H_2OCbl^+ (pH 5), HOCbl (pH 9), and $(H_2O)_2Cbi^{2+}$ are compared in Figure 3 (top panel). All three species exhibit so-called "typical" corrinoid Abs spectra characterized by a prominent feature in the visible region, which exhibits a partially resolved vibrational progression that includes the α- and β-bands, and an intense feature centered in the UV region, designated as the γ-band. Upon the addition of a buffered solution of CobA, the Abs spectrum of H_2OCbl^+ changes significantly; both the α- and γ-bands decrease in intensity and red-shift by 400 and 470 cm^{-1}, respectively (cf. Figure 3A,D). However, these spectral changes can be attributed primarily to deprotonation of the cobalamin to yield HOCbl (cf. Figure 3B), as the protein solution was buffered to a pH of 8.0 while the pK_a of the water ligand of free H_2OCbl^+ is 7.6.[41] Interestingly, though, a new feature is observed at 21 200 cm^{-1} that has no counterpart in the Abs spectrum of any Co^{3+}corrinoid. This feature is reminiscent of the α-band of Co^{2+}corrinoids (vide infra), suggesting that the presence of 20 mM dithiothreitol (DTT) in the buffer caused partial reduction of the corrinoid to $Co^{2+}Cbl$.

H_2OCbl^+ + CobA/ATP. The Abs spectrum of H_2OCbl^+ in the presence of the CobA/ATP complex is almost identical to that of H_2OCbl^+/CobA (cf. Figure 3D,E). This result suggests that the presence of ATP in the CobA active site has little effect on the electronic structure of the bound Co^{3+}corrinoid substrate or that H_2OCbl^+ does not actually bind to the enzyme. Nevertheless, the relative intensity of the Abs feature at 21 200 cm^{-1} attributed to the α-band of Co^{2+}corrinoid increases by 12% when ATP is present, possibly suggesting that reduced cobalamin is more readily bound, and thus protected against reoxidation, when CobA is complexed with ATP.

3.2. Co^{2+}Corrinoid↔CobA Interaction. (i) Abs and MCD. Similar to the case of Co^{3+}corrinoids, the energy of the α-band transition of Co^{2+}corrinoids (involving the same pair of cor π/π^*-based donor and acceptor MOs as the α-band transition of Co^{3+}corrinoids) is also sensitive to the identity of the lower ligand, undergoing a 150 cm^{-1} blue-shift upon substitution of the DMB ligand of $Co^{2+}Cbl$ with a water molecule to yield $Co^{2+}Cbi^+$ (cf. Figures 4A and 5A).[20] Both $Co^{2+}Cbl$ and Co^{2+}-Cbi^+ are paramagnetic ($S = {}^1/_2$) species and give rise to richly structured, temperature-dependent MCD spectra. Detailed analyses of these spectra within the framework of TD-DFT calculations revealed that electronic transitions can be classified as being either Co^{2+} ligand field (LF), $Co^{2+}\rightarrow$cor π^* charge transfer (CT), or cor $\pi\rightarrow\pi^*$ in nature (Figure 4A). On the basis

(41) Kratky, C.; Farber, G.; Gruber, K.; Wilson, K.; Dauter, Z.; Nolting, H. F.; Konrat, R.; Kräutler, B. *J. Am. Chem. Soc.* **1995**, *117*, 4654−4670.

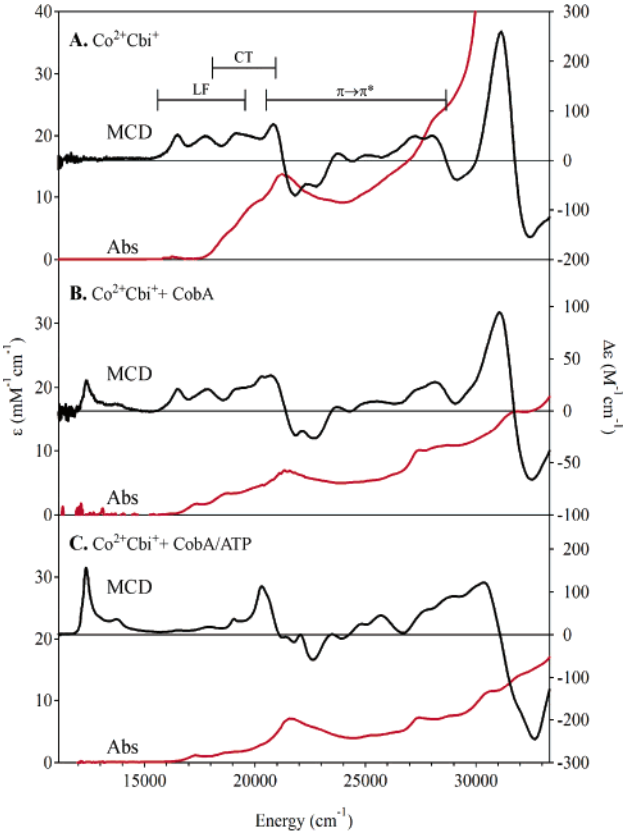

Figure 5. Abs (red traces, left axis) and 7 T MCD (black traces, right axis) spectra recorded at 4.5 K of (A) free $Co^{2+}Cbi^{+}$, (B) $Co^{2+}Cbi^{+}$ in the presence of CobA, and (C) $Co^{2+}Cbi^{+}$ in the presence of the CobA/ATP complex.

of these assignments, changes in spectral features upon corrinoid binding to CobA can be analyzed in terms of molecular perturbations so as to determine possible modes of activation of Co^{2+}Cbl for further reduction.

Co^{2+}Cbl + CobA. The Abs spectrum of Co^{2+}Cbl in the presence of a slight excess of CobA (Figure 4B) is qualitatively similar to that of free Co^{2+}Cbl (Figure 4A). Although the latter spectrum exhibits slightly increased intensity around 18 000 cm^{-1}, this difference can be ascribed to a small fraction of oxidized cobalamin (i.e., HOCbl). While Abs spectroscopy alone yields little insight into the nature of the interaction between Co^{2+}Cbl and CobA, low-temperature MCD spectroscopy provides a much more sensitive probe of this interaction. Comparison of the MCD spectra in Figure 4A,B reveals only small differences in intensity distribution throughout the CT and cor $\pi\rightarrow\pi^*$ spectral regions. Notably, both the LF transition energies and the α-band position are virtually identical for the free and CobA-bound Co^{2+}Cbl species, precluding any significant perturbation of the Co^{2+} coordination environment in the enzyme active site.

Co^{2+}Cbl + CobA/ATP. In contrast to the rather modest spectral changes accompanying Co^{2+}Cbl binding to substrate-free CobA described above, a significant blue-shift ($\Delta = 450$ cm^{-1}) of the α-band to 21 550 cm^{-1} is observed in the Abs spectrum of Co^{2+}Cbl upon the addition of CobA that was incubated with a 20-fold excess of the co-substrate ATP (Figure 4C). Likewise, the corresponding MCD spectrum exhibits pronounced differences in signal intensity throughout the entire spectral region (in particular, near 18 000 and 28 000 cm^{-1}) compared to the free Co^{2+}Cbl spectrum. Most striking, however, is the appearance of a temperature-dependent MCD feature at 12 400 cm^{-1}. Because this feature has no obvious counterpart in the Abs spectrum (Figure 4C), it can attributed to an LF transition of Co^{2+}, as transitions of this type are formally electric dipole forbidden.[42] The shift in α-band energy coupled with the appearance a new LF transition suggests that the presence of ATP in the CobA active site triggers significant changes in the Co^{2+} coordination environment.

$Co^{2+}Cbi^{+}$ + CobA. In an attempt to obtain further insight into the nature of the paramagnetic species responsible for the MCD feature at 12 400 cm^{-1} in the spectrum of Co^{2+}Cbl + CobA/ATP (Figure 4C), the spectroscopic studies described above were repeated with Co^{2+}cobinamide ($Co^{2+}Cbi^{+}$), a precursor of Co^{2+}Cbl that lacks the nucleotide loop (Figure 1). Comparison of the Abs spectra of free $Co^{2+}Cbi^{+}$ (Figure 5A) and $Co^{2+}Cbi^{+}$ in the presence of substrate-free CobA (Figure 5B) reveals a small blue-shift ($\Delta = 100$ cm^{-1}) of the α-band to 21 350 cm^{-1} in the latter spectrum. Additional Abs features at 17 350 and 18 700 cm^{-1} coincide with the α- and *β*-bands of the $(H_2O)_2Cbi^{2+}$ starting material (see Figure 3C), signaling that some reoxidation of the Co^{2+}corrinoid species occurred (as for Co^{2+}Cbl, vide supra). Inspection of the corresponding low-temperature MCD spectra (Figure 5A,B) reveals that, in fact, two paramagnetic species are present in the $Co^{2+}Cbi^{+}$ + CobA sample. The dominant component exhibits spectral features nearly identical to those of unbound $Co^{2+}Cbi^{+}$, suggesting that substrate-free CobA does not significantly interact with Co^{2+}-Cbi^{+}, as well. However, the appearance of the MCD feature at 12 400 cm^{-1} indicates that some portion of $Co^{2+}Cbi^{+}$ is converted to a species similar to that observed in the MCD spectrum of Co^{2+}Cbl bound to the CobA/ATP complex (Figure 4C).

$Co^{2+}Cbi^{+}$ + CobA/ATP. As noted above for Co^{2+}Cbl, the Abs spectrum of $Co^{2+}Cbi^{+}$ is also greatly altered upon corrinoid binding to the CobA/ATP complex (cf. Figure 5A,C). Most notably, the α-band shifts to 21 550 cm^{-1}, which is similar to the position of the α-band in the spectrum of Co^{2+}Cbl obtained under identical conditions (Figure 4C). The low-temperature MCD spectrum of the $Co^{2+}Cbi^{+}$ + CobA/ATP sample (Figure 5C) is completely unprecedented, being dominated entirely by features that have no counterparts in the spectrum of any unbound Co^{2+}corrinoid studied to date.[20] On the basis of their large MCD-to-Abs intensity ratios, the transitions at 12 400, 13 700, and 19 000 cm^{-1} are readily assigned as LF transitions. In comparison, the features appearing between 21 100 and 30 000 cm^{-1} have much smaller MCD-to-Abs intensity ratios; thus, they are attributed to CT and cor $\pi\rightarrow\pi^*$ transitions.[43] The striking perturbation of the LF transitions when the free Co^{2+}-corrinoids (Figures 4A and 5A) bind to the CobA/ATP complex can only be rationalized by a dramatic change in the coordination environment of the initially five-coordinate Co^{2+} center. To interpret these spectral changes in terms of molecular perturbations, it is important to note that all MCD features attributed to LF transitions are positively signed in both the free and the CobA/ATP-bound $Co^{2+}Cbi^{+}$ spectra (Figure 5A,C). Alterna-

(42) Pavel, E. G.; Solomon, E. I. In *Spectroscopic Methods in Bioinorganic Chemistry*; Solomon, E. I., Hodgson, K. O., Eds.; American Chemical Society: Washington, DC, 1998; pp 119−135.
(43) The weak MCD features at 17 000 and 18 000 cm^{-1} are due to residual unbound $Co^{2+}Cbi^{+}$.

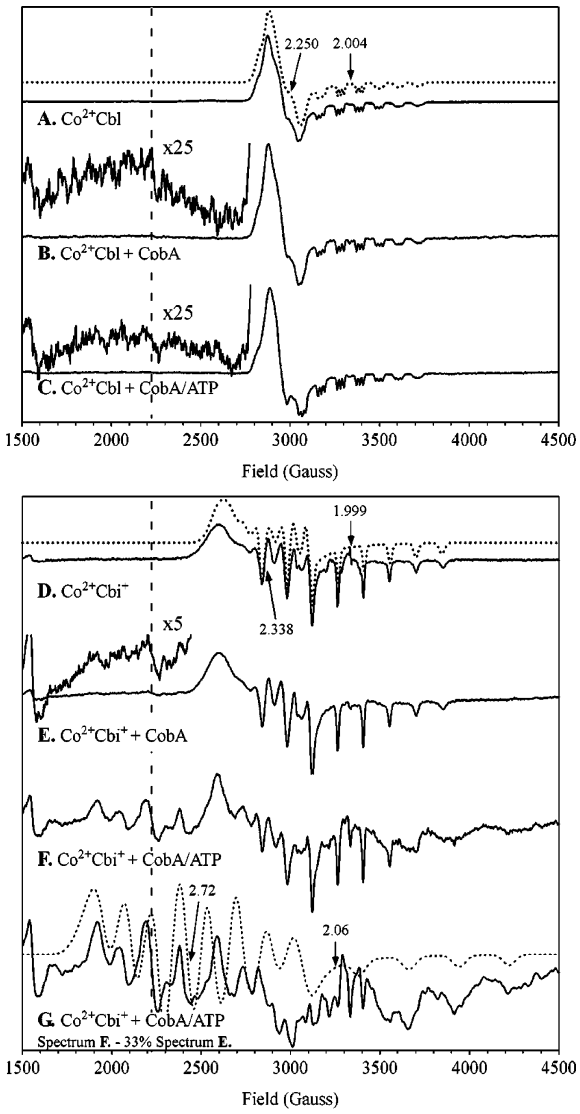

Figure 6. Top panel: X-band EPR spectra collected at 40 K of (A) free Co^{2+}Cbl, (B) Co^{2+}Cbl in the presence of CobA, and (C) Co^{2+}Cbl in the presence of the CobA/ATP complex. Bottom panel: EPR spectra at 40 K of (D) free $Co^{2+}Cbi^{+}$, (E) $Co^{2+}Cbi^{+}$ in the presence of CobA, and (F) Co^{2+}-Cbi^{+} in the presence of the CobA/ATP complex. All Co^{2+}corrinoid species were prepared by BH_4^- reduction in 50 mM TRIS buffer (pH 8.0). EPR spectra were collected using 9.36 GHz microwave frequency, 8.0 mW microwave power, 5.2 G modulation amplitude, 100 kHz modulation frequency, and 328 ms time constant. Spectrum G was obtained by subtracting 33% of spectrum E from spectrum F. Spectra were simulated (dotted lines) using the parameters given in Table 1.

tively, in the case of Co^{2+}Cbl, an almost even distribution of positively and negatively signed MCD features associated with the LF transitions is observed (Figure 4A). The dominance of positive signal intensity exhibited by the $Co^{2+}Cbi^{+}$ MCD spectra is characteristic of low-lying excited states mixing into the ground state via spin−orbit coupling. The fact that this excess positive intensity persists upon binding of $Co^{2+}Cbi^{+}$ to the CobA/ATP complex indicates that the resulting species also possesses (a) low-lying excited state(s), consistent with a weak axial LF component experienced by the Co^{2+} center in the protein-bound corrinoid. Moreover, the presence of the 12 400 cm^{-1} feature in all MCD spectra of CobA-bound Co^{2+}corrinoids discussed above implies that the nature of the unique Co^{2+}-corrinoid species that is generated in the CobA/ATP active site is largely independent of the identity of the lower axial ligand in the free corrinoid substrate.

(ii) EPR. MCD experiments described above were complemented with EPR studies, as this technique provides a uniquely sensitive probe of the axial ligation of Co^{2+}corrinoids. X-band (9.36 GHz) EPR spectra recorded at 40 K for all Co^{2+}corrinoid samples described above are presented in Figure 6.[44] The addition of substrate-free CobA to a solution containing Co^{2+}-Cbl has no major effect on the corresponding EPR spectrum but nonetheless causes a minor sharpening of the axial nitrogen superhyperfine features centered at 3400 G (Figure 6B), suggesting that the $Co-N_{ax}$ bond is more constrained in the protein active site. Interestingly, this sharpening becomes much more pronounced when ATP-bound rather than substrate-free CobA is added to the Co^{2+}Cbl solution (Figure 6C), allowing for the resolution of ^{14}N superhyperfine splittings on all but the highest field feature.

The EPR spectrum of $Co^{2+}Cbi^{+}$ bound to substrate-free CobA (Figure 6E) is nearly identical to that of the free corrinoid (Figure 6D), the exception being the appearance of a small derivative-shaped feature at 2200 G. Importantly, the metal hyperfine splitting remains unchanged, and furthermore, no additional fine structure appears that would signal axial coordination of an atom possessing a nuclear magnetic moment (e.g., ^{14}N, $I = 1$). This finding precludes that upon corrinoid binding to CobA, an active site histidine residue displaces the H_2O ligand, a binding scheme employed by several B_{12}-dependent enzymes.[45−48] While the spectral changes induced by binding $Co^{2+}Cbi^{+}$ to substrate-free CobA are rather insignificant, much more dramatic perturbations to the EPR spectrum are observed when ATP-bound CobA is used instead (Figure 6F). The series of sharp negative resonances in this spectrum centered at $g = 2.00$ and split by 140 G indicate that some of the $Co^{2+}Cbi^{+}$ does not interact strongly with the CobA/ATP complex (possibly reflecting a sizable population of unbound corrinoid); this contribution was removed by subtracting the suitably scaled ($\times 0.33$) $Co^{2+}Cbi^{+}$ + CobA spectrum (Figure 6E) to obtain the trace shown in Figure 6G. Simulation of the resulting spectrum requires nearly axial g values and unusually large ^{59}Co hyperfine parameters $A(^{59}Co)$ (Table 1). Not surprisingly, given the uniqueness of the MCD spectrum exhibited by this species (Figure 5C), such EPR parameters had never before been reported for any Co^{2+}corrinoid species. The implications of these results with respect to the molecular structure of $Co^{2+}Cbi^{+}$ bound to the CobA/ATP complex will be explored in 3.4. Spectro/Structural Correlation.

3.3. AdoCbl↔CobA Interaction. Abs, CD, and MCD spectra of free AdoCbl and AdoCbl in the presence of ATP-bound CobA are presented in Figure 7. While the two data sets are nearly indistinguishable, the addition of the CobA/ATP complex to a solution of the AdoCbl product causes a sharpening

(44) As the EPR spectra of free Co^{2+}Cbl (Figure 6A) and $Co^{2+}Cbi^{+}$ (Figure 6D) are essentially identical to previously published data (EPR parameters are listed in Table 1), it can be concluded that neither the buffer nor the presence of ATP in the solution has any effect on the Co^{2+}corrinoid spectral properties. The small negative feature at 3250 G ($g = 2.00$) is due to a minor Cu^{2+} impurity that resides in the EPR cavity. Collecting high temperature (40 K) data minimizes this contribution to the EPR spectra.

(45) Drennan, C. L.; Huang, S.; Drummond, J. T.; Matthews, R. G.; Ludwig, M. L. *Science* **1994**, *266*, 1669−1674.
(46) Padmakumar, R.; Banerjee, R. *J. Biol. Chem.* **1995**, *270*, 9295−9300.
(47) Reitzer, R.; Gruber, K.; Jogl, G.; Wagner, U. G.; Bothe, H.; Buckel, W.; Kratky, C. *Structure* **1999**, *7*, 891−902.
(48) Chang, C. H.; Frey, P. A. *J. Biol. Chem.* **2000**, *275*, 106−114.

Table 1. Experimental and EPR Parameters for Selected Co^{2+}Corrinoids and Synthetic Co^{2+}-Containing Macrocyclic Complexes

species	g_z	g_y	g_x	$A(^{59}Co)$, MHz A_z	A_y	A_x
free Co^{2+}Cbl	2.004	2.230	2.280	305	30	40
free $Co^{2+}Cbi^{+}$	1.999	2.338	2.338	405	220	220
$Co^{2+}Cbi^{+}$ + CobA/ATP	2.06	2.67	2.73	805	590	635
$[Co(Me_6[14]dieneN_4)(H_2O)]$[a]	2.016	2.43	2.43	375		
Co^{2+}(OEP)[b]	1.944	2.890	2.816	408	705	653
α-Co^{2+}Pc[c]	2.007	2.422	2.422	348	197	197
β-Co^{2+}Pc[d]	1.89	2.94	2.94	480	780	809

[a] Five-coordinate ($Co-OH_2$ distance of 2.315 Å) (ref 49). [b] Four-coordinate Co^{2+}octaethylporphyrin (OEP) doped into $C_{70}{\cdot}Ni^{2+}$(OEP)$\cdot C_6H_6\cdot CHCl_3$ host crystal (ref 55). [c] Four-coordinate (nearest neighbor at 3.8Å Co^{2+}phthalocyanine (Pc) doped into α-Zn^{2+}Pc (ref 56). [d] Four-coordinate (nearest neighbor at 3.38 Å) Co^{2+}phthalocyanine (Pc) doped into β-Zn^{2+}Pc (ref 56).

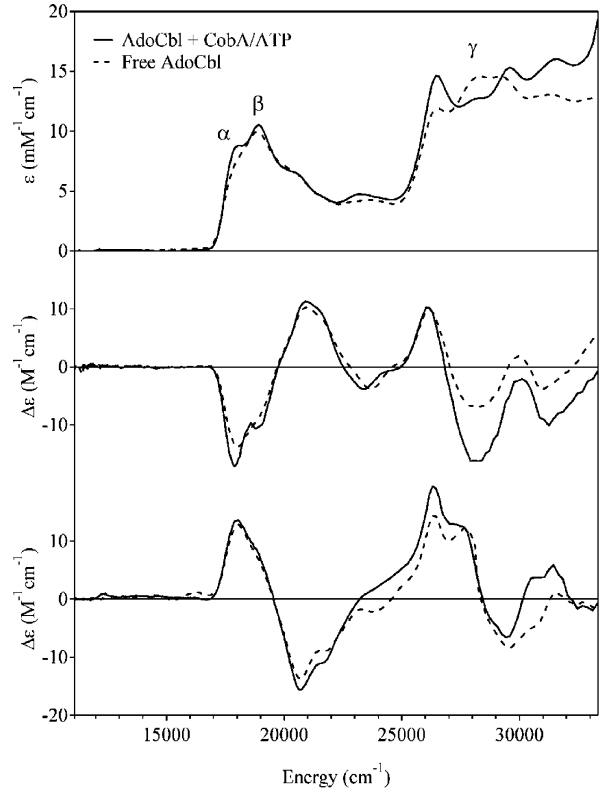

Figure 7. Abs (top), CD (center), and 7 T MCD (bottom) spectra recorded at 4.5 K of AdoCbl in the presence of the CobA/ATP complex (solid line) and of free AdoCbl (broken line).

and slight increase in the intensity of the α- and β-bands (at 17 950 and 19 000 cm^{-1}, respectively). More pronounced differences are evident in the so-called γ-region (near 27 000 cm^{-1}) where several cor $\pi\rightarrow\pi^*$ transitions contribute to the Abs envelope.[19] Similar spectral changes were observed upon binding of AdoCbl to apo-MMCM, results that were attributed to the imposition of a strict conformation on the Ado moiety and a decreased local dielectric constant in the enzyme active site.[21] Collectively, these findings suggest that AdoCbl does bind to the CobA/ATP complex, albeit without undergoing significant geometric and electronic changes.

3.4. Spectro/Structural Correlation. The spectroscopic data presented above indicate that a unique Co^{2+}corrinoid species is generated when either Co^{2+}Cbl or $Co^{2+}Cbi^{+}$ binds to the CobA/ATP complex. This finding is not necessarily surprising considering that CobA must somehow activate the Co^{2+}corrinoid substrate so as to facilitate its reduction to the Co^{1+} state. One way such an activated species may be generated in the enzyme active site is through manipulation of the lower ligand bonding interaction, as this would provide a means for a direct modulation of the energy of the redox-active Co d_{z^2}-based molecular orbital (MO). To test this hypothesis, DFT and TD-DFT calculations were performed on $Co^{2+}Cbi^{+}$ models differing with respect to their lower ligand bond length. The $Co-OH_2$ coordinate was systematically varied from 2.100 to 2.650 Å, and for each configuration, the corresponding Abs spectrum and EPR parameters were computed.

Table 2. Selected Experimental and Calculated LF Transition Energies (in cm^{-1}) for $[Co(Me_6[14]dieneN_4)(H_2O)$

exp[a]	TD-DFT	INDO/S-CI[b]	Slater[b]	assignment
5900	12300	3119	4875	$d_{xz}\rightarrow d_{z^2}$
5900	13125	3556	5125	$d_{yz}\rightarrow d_{z^2}$
13500	20725	11502	12975	$d_{xy}\rightarrow d_{z^2}$

[a] Refs 25 and 49. [b] See Supporting Information for computational details.

(i) Validation of Computational Approach and Implications for $Co^{2+}Cbi^{+}$ Spectral Assignments. To validate the use of the computational approach described above for the prediction of $Co^{2+}Cbi^{+}$ LF transition energies and *g* values as a function of the $Co-OH_2$ distance, we also performed DFT and TD-DFT calculations on the well-characterized Co^{2+} complex *N-rac*-[Co^{2+}-5,7,7,12,14,14-hexamethyl-1,4,8,11-tetraazacyclotetradeca-4,11-diene(H_2O)], hereafter referred to as $[Co(Me_6[14]dieneN_4)(H_2O)]$ (Scheme 1).[25] This complex was chosen for its structural similarity to $Co^{2+}Cbi^{+}$, as the metal center is ligated equatorially by a tetradentate N-based ligand ($Me_6[14]dieneN_4$) that mimics the corrin ring and also possesses an axially bound water molecule with a $Co-OH_2$ bond distance of 2.315 Å. Magnetic susceptibility and EPR experiments on $[Co(Me_6[14]dieneN_4)(H_2O)]$ demonstrated that this complex is low-spin ($S = {}^1/_2$) and indicated that the unpaired electron resides in the Co $3d_{z^2}$-based MO.[49] Consistent with these experimental findings, our DFT calculations carried out on a complete model of $[Co(Me_6[14]dieneN_4)(H_2O)]$ predict a Co $(3d_{z^2})^1$ ground state electron configuration. Selected LF transition energies computed using TD-DFT are presented in Table 2, along with published experimental results from near-IR Abs studies.[25,49] This comparison reveals that the BP TD-DFT method overestimates the energy of these LF transitions by ~6500 cm^{-1}. Interestingly, the predicted energies for $[Co(Me_6[14]dieneN_4)(H_2O)]$ are similar to those computed previously for the "unperturbed" $Co^{2+}Cbi^{+}$ model (cf. Table S5), suggesting that the $Co^{2+}Cbi^{+}$ LF transition energies are also overestimated by ~6500 cm^{-1}. This hypothesis is supported by the fact that much lower LF excited state energies are computed for both the $Co^{2+}Cbi^{+}$ and $[Co(Me_6[14]dieneN_4)(H_2O)]$ models by using the semiempirical intermediate neglect of differential overlap (INDO/S-CI)[50,51] or Slater half-electron excitation methods[52] (Tables 2 and S5), computational approaches that have been used with considerable success in past studies of bioinorganic systems. Importantly,

(49) Goedken, V. L.; Kjeldahl, N. K.; Busch, D. H. *J. Coord. Chem.* **1977**, *7*, 89−103.
(50) Ridley, J.; Zerner, M. C. *Theor. Chim. Acta* **1973**, *32*, 111−134.
(51) Zerner, M. C.; Loew, G. H.; Kirchner, R. F.; Mueller-Westerhof, U. T. *J. Am. Chem. Soc.* **1980**, *102*, 589−599.
(52) Slater, J. C. *The Calculation of Molecular Orbitals*; John Wiley & Sons: New York, 1979.

Table 3. Experimental and Calculated EPR Parameters for $[Co(Me_6[14]dieneN_4)(H_2O)$

				$A(^{59}Co)$, MHz		
	g_z	g_y	g_x	A_z	A_y	A_x
exp[a]	2.016	2.43	2.43	375		
CP-SCF	2.006	2.103	2.121	650	258	244
ZORA[b]	1.948	2.381	2.662	1025	558	517

[a] Ref 49. [b] See Supporting Information for computational details.

regardless of the method used, our calculations consistently predict similar LF transition energies for $Co^{2+}Cbi^+$ and $[Co(Me_6[14]dieneN_4)(H_2O)]$ (cf. Tables S5 and S6). Therefore, it is likely that the Co^{2+} $d_{xz}\rightarrow d_{z^2}$ and $d_{yz}\rightarrow d_{z^2}$ transitions of Co^{2+}-Cbi^+ lie outside the range accessible to our MCD instrument, and that the observed lowest energy transition for this species (Figure 5A) formally involves excitation of an electron from the Co $3d_{xy}$-orbital to the singly occupied d_{z^2}-orbital.

Comparison of the experimental and CP-SCF computed EPR parameters for the $[Co(Me_6[14]dieneN_4)(H_2O)]$ model indicates that g_x and g_y are significantly underestimated relative to their experimental values (Table 3). Additionally, the ^{59}Co hyperfine parameters, which provide a measure of the unpaired spin density on the metal nucleus, are considerably overestimated by the CP-SCF method. In an attempt to improve upon these results, EPR g values were also calculated using the zeroth-order regular approximation (ZORA) to the Hamiltonian;[53,54] however, these computations yielded no significant improvement over those employing CP-SCF DFT (Table 3). Collectively, these results indicate that DFT-based computational approaches fail at reliably predicting EPR parameters of Co^{2+}corrinoid-like systems. Therefore, the g values and ^{59}Co hyperfine parameters derived from the experimental EPR spectrum of $Co^{2+}Cbi^+$ bound to the CobA/ATP complex (Figure 6G) were interpreted within the framework of spectral correlations to well-characterized Co^{2+}-containing macrocyclic systems (see Effects on EPR Parameters below).

(ii) Effects on Abs Spectrum. To examine the effects of perturbations along the axial coordinate on the excited state electronic structure of $Co^{2+}Cbi^+$, TD-DFT was used to compute the Abs spectra for a series of $Co^{2+}Cbi^+$ models with differing $Co-OH_2$ bond lengths (Figure 8A). These computations predict that the dominant feature in the visible region (the α-band) blue-shifts by $\sim$15 cm^{-1}/pm as the $Co-OH_2$ bond length is increased from its equilibrium value of 2.201 Å. While the donor MO involved in the corresponding transition is mostly cor π-based, it also possesses significant (37%) Co $3d_{z^2}$-orbital character as well as a small contribution (2%) from an oxygen-based lone pair of the H_2O ligand, making it weakly $Co-OH_2$ σ-antibonding. Thus, the blue-shift of the α-band with increasing $Co-OH_2$ bond length can be understood in terms of a weakening of this σ-antibonding interaction.

Yet, it is primarily the perturbation of the LF transitions, which carry little intensity in the Abs spectrum, that gives rise to the massive differences between our experimental MCD spectra (Figures 4 and 5). As a weakening of the $Co-OH_2$ σ-antibonding interaction stabilizes MOs with significant Co $3d_{z^2}$-orbital character, LF transitions originating from these

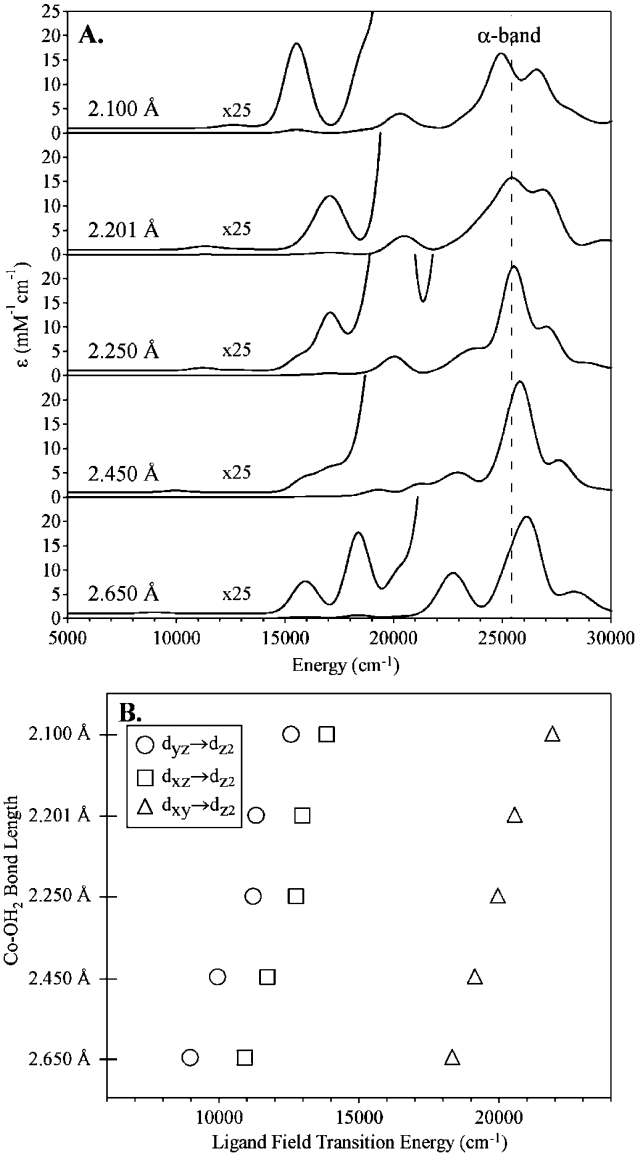

Figure 8. (A) TD-DFT computed Abs spectra for a series of $Co^{2+}Cbi^+$ models that differ with respect to the lower axial ligand bond length. The $Co-OH_2$ bond lengths are given on the left, and the peak position of the α-band in the computed spectrum for the unperturbed model ($Co-OH_2$ bond length of 2.201 Å) is indicated by a vertical dotted line for reference. (B) Evolution of TD-DFT computed energies of selected LF transitions (symbols) as a function of the $Co-OH_2$ bond length.

orbitals exhibit considerable blue-shifts with increasing lower ligand bond length. Alternatively, LF transitions that terminate in the Co $3d_{z^2}$-based spin-down LUMO display large red-shifts in response to $Co-OH_2$ bond lengthening. This prediction that some transitions shift toward lower energy upon weakening of the lower ligand bonding interaction is verified by our TD-DFT results (Figure 8B) and provides a rationale for the red-shift (to 12 400 cm^{-1}) of the experimentally observed lowest energy MCD feature, assigned to the Co^{2+} $d_{xy}\rightarrow d_{z^2}$ transition, upon $Co^{2+}Cbi^+$ binding to the CobA/ATP complex (Figure 5A,C).

(iii) Effects on EPR Parameters. As demonstrated in the previous section, elongation of the $Co-OH_2$ bond of $Co^{2+}Cbi^+$ causes significant shifts of the LF transitions. Molecular g values are predicted to be similarly sensitive to distortions along this coordinate, as stabilization of the Co $3d_{z^2}$-based MO allows for more efficient mixing via spin−orbit coupling of the Co^{2+}

(53) van Lenthe, E.; Snijders, J. G.; Baerends, E. J. *J. Chem. Phys.* **1996**, *105*, 6505−6516.
(54) van Lenthe, E.; van der Avoird, A.; Wormer, P. E. S. *J. Chem. Phys.* **1998**, *108*, 4783−4796.

$d_{xz} \rightarrow d_{z^2}$ and $d_{yz} \rightarrow d_{z^2}$ excited states into the ground state, thereby causing g_x and g_y to shift further away from the free electron value (Table S10). Furthermore, lengthening the lower ligand bond reduces the Co−OH_2 bond covalency, thus giving rise to increased unpaired spin density on the Co center. These qualitative predictions concur nicely with the dramatic changes in g values and ^{59}Co hyperfine parameters observed by EPR spectroscopy when $Co^{2+}Cbi^+$ binds to the CobA/ATP complex (Table 1, Figure 6G). Collectively, these results hint toward a description of the enzyme-bound species as an essentially four-coordinate square-planar Co^{2+} complex with, perhaps, a weakly interacting oxygen-based axial ligand. Strong support for this description is provided by the strikingly similar appearance of the EPR spectrum in Figure 6G and those reported for Co^{2+}-porphyrins[55] and Co^{2+}pthalocyanines[56] that are rigorously four-coordinate (square-planar) or weakly bind a solvent (e.g., H_2O) molecule in the axial position. EPR parameters for representative members of these two classes of synthetic Co^{2+} complexes are included in Table 1.

4. Discussion

Considerable research effort has been directed toward elucidating the geometric and electronic factors contributing to the remarkable activation of the Co−C bond of AdoCbl (Figure 1) for homolysis by B_{12}-dependent enzymes.[57−62] In contrast, the biological formation of this unique organometallic bond that lies at the heart of the reactivity of the coenzyme B_{12} has attracted relatively little attention.[12,22,63] In this study, we have built upon the foundation established in our earlier characterization of free Co^{3+}- and Co^{2+}corrinoids to analyze changes in Abs and MCD spectroscopic data of physiologically relevant precursors of AdoCbl as they interact with the bacterial adenosyltransferase CobA. Key insights gained from these studies are summarized below, and their possible implications for the mechanism of $Co^{2+} \rightarrow Co^{1+}$ reduction employed by Co−C bond-forming enzymes are explored.

Corrinoid↔CobA Interactions. (i) Co^{3+}Corrinoids. Abs and CD spectra of H_2OCbl^+ in the presence of CobA (Figures 3D and S2) are different from those of unbound H_2OCbl^+ (Figures 3A and S1), yet similar to those of free HOCbl (Figures 3B and S1), as expected considering that the protein-containing sample was sufficiently basic (pH 8.0) to promote deprotonation of the upper axial H_2O ligand of H_2OCbl^+ (pK_a of 7.6).[41] The only notable difference between the H_2OCbl^+/CobA and unbound HOCbl data sets is the presence of an additional feature at ∼21 100 cm^{-1} in the former, attributed to base-on Co^{2+}Cbl on the basis of corresponding MCD data (cf. Figures 4A and S2). Analogous spectroscopic studies of H_2OCbl^+ in the presence of the CobA/ATP complex provide nearly identical results, also revealing that the cobalamin cofactor is converted to HOCbl and that a significant portion is reduced to the Co^{2+} oxidation state. Interestingly, however, a modest (∼12%) increase in the yield of HOCbl conversion to Co^{2+}Cbl is observed when co-substrate ATP is present in the CobA active site, suggesting that the CobA/ATP complex has a higher affinity for Co^{2+}Cbl and/or raises the $Co^{3+/2+}$ reduction potential relative to the ATP-free form of the enzyme.

While the results described above are not conclusive as to whether Co^{3+}corrinoids actually bind to the CobA active site, the small but notable spectral changes observed upon the addition of ATP-bound CobA to a solution of AdoCbl (Figure 7) indicate that CobA does indeed interact with Co^{3+}corrinoids. In particular, the increased Abs intensity in the γ-region is characteristic of a decrease in the dielectric constant resulting from the exclusion of water from the local environment of the cofactor, consistent with the crystallographic observation of an N-terminal α-helix of CobA that is properly positioned to seal off the active site from bulk solvent.[9] Importantly, while some bands in the γ-region exhibit minor changes in peak position and intensity, the α- and β-bands are not perturbed to any significant degree. On the basis of our previous spectro/structural correlation studies of alkyl-Co^{3+}corrinoids,[21] this observation definitively precludes any strong protein interaction with the axial ligands and, ultimately, is consistent with the need for CobA to readily dissociate the product.

(ii) Co^{2+}Corrinoids. On the basis of the close resemblance of the corresponding MCD spectra (Figure 4), the geometric and electronic structures of Co^{2+}Cbl are not significantly perturbed when this species binds to CobA, indicating that the lower ligand coordination by DMB is maintained in the enzyme active site. However, in the presence of co-substrate ATP, a small portion (∼10%) of the Co^{2+}Cbl substrate is converted to an unprecedented paramagnetic species characterized by a LF transition with positively signed, prominent MCD intensity at 12 400 cm^{-1}. As this feature is not present in the MCD spectrum of free $Co^{2+}Cbi^+$ (Figure 5A), the spectral changes that accompany binding of Co^{2+}Cbl to CobA cannot be rationalized solely in terms of a protein-induced replacement of the DMB with a water molecule (a scenario uncovered recently for hATR).[64] When substrate-free CobA is treated with $Co^{2+}Cbi^+$, the same unique paramagnetic species is formed, albeit in greater yield (Figure 5B). With ATP also bound to the CobA active site, $Co^{2+}Cbi^+$ is almost completely converted to this new species (Figure 5C), allowing for a full spectroscopic characterization of this putative Co^{2+}corrinoid/CobA intermediate. Our data indicate that this species exhibits a unique set of LF transitions that dominate the near-IR region of the MCD spectrum, as well as a blue-shifted α-band Abs feature (by 450 cm^{-1}), signifying a weakened interaction between the Co 3d-orbitals and the cor π-based frontier MOs.[20]

The EPR spectrum of the $Co^{2+}Cbi^+$/CobA/ATP ternary complex (Figure 6G) indicates that 67% of the corrinoid substrate converts to a new species characterized by g values and ^{59}Co A parameters that are strikingly different from those reported for any free Co^{2+}corrinoid (Figure 6, Table 1). Quantitative analysis of the corresponding EPR spectrum yields $g_\perp$ values (∼2.7) and components of the ^{59}Co hyperfine tensor

(55) Ozarowski, A.; Lee, H. M.; Balch, A. L. *J. Am. Chem. Soc.* **2003**, *125*, 12606−12614.
(56) Assour, J. M.; Kahn, W. K. *J. Am. Chem. Soc.* **1965**, *87*, 207−212.
(57) Chowdhury, S.; Banerjee, R. *Biochemistry* **2000**, *39*, 7998−8006.
(58) Andruniow, T.; Zgierski, M. Z.; Kozlowski, P. M. *Chem. Phys. Lett.* **2000**, *331*, 509−512.
(59) Dong, S. L.; Padmakumar, R.; Banerjee, R.; Spiro, T. G. *J. Am. Chem. Soc.* **1999**, *121*, 7063−7070.
(60) Hay, B. P.; Finke, R. G. *J. Am. Chem. Soc.* **1986**, *108*, 4820−4829.
(61) Mealli, C.; Sabat, M.; Marzilli, L. G. *J. Am. Chem. Soc.* **1987**, *109*, 1593−1594.
(62) Calafat, A. M.; Taoka, S.; Puckett, J. M.; Semerad, C.; Yan, H.; Luo, L. B.; Chen, H. L.; Banerjee, R.; Marzilli, L. G. *Biochemistry* **1995**, *34*, 14125−14130.
(63) Sato, K.; Nakashima, T.; Shimizu, S. *J. Nutr. Sci. Vitaminol.* **1984**, *30*, 405−413.
(64) Yamanishi, M.; Labunska, T.; Banerjee, R. *J. Am. Chem. Soc.* **2005**, *127*, 526−527.

(~800 and ~600 MHz for $A_{||}$ and $A_{\perp}$, respectively) that are unusually large for a Co^{2+}corrinoid; however, these parameters are in fact remarkably similar to those reported for Co^{2+}-porphyrins[55] and Co^{2+}pthalocyanines[56] (Table 1), wherein the lower ligand is considerably removed from the Co^{2+} ion or is completely absent. Consequently, it is tempting to speculate that the Co^{2+}corrinoid species present in the CobA/ATP complex is significantly perturbed with respect to this lower ligand coordinate. Support for this proposal is provided by the Co^{2+}-Cbi^{+} spectro/structural correlation developed in this work. Specifically, our computations predict that a 0.3 Å elongation of the $Co-OH_2$ bond will blue-shift the α-band maximum by ~500 cm^{-1}, red-shift the $d_{xy}\rightarrow d_{z^2}$ LF transition by ~3000 cm^{-1} (Figure 8), and substantially raise the $g_{\perp}$ values (Table S10), all in striking agreement with our experimental data. These massive changes in spectroscopic properties primarily reflect the decrease in $Co-OH_2$ σ-antibonding interaction and consequent stabilization of the Co $3d_{z^2}$-orbital in response to a partial dissociation of the lower axial ligand. Collectively, our results strongly suggest that the species responsible for the unique MCD and EPR spectral features observed for CobA-containing samples of Co^{2+}Cbl and $Co^{2+}Cbi^{+}$ is best described as possessing an essentially four-coordinate Co^{2+} center that lacks any significant axial bonding interactions. Possible implications of this remarkable finding for the function of CobA are explored in the next section.

Activation Mechanism for Corrinoid Reduction Employed by CobA. It has been shown that Flavodoxin A (FldA) is a flavin mononucleotide (FMN)-dependent electrontransferase that serves as the terminal member of a system of enzymes designed to harness the reducing power of NADH and is capable of providing the electron required for the $Co^{2+}\rightarrow Co^{1+}$ reduction in the CobA active site (Figure 2).[65] A most intriguing aspect of this reaction is that the one-electron reduction of free Co^{2+}-Cbl is physiologically unfeasible, as the corresponding midpoint potential ($E^{\circ} = -610$ mV vs SHE)[17] is much lower than that of FldA ($E^{\circ} = -440$ mV for the semiquinone/reduced FMN couple[18]); therefore, for this reduction to become thermodynamically favorable, CobA must suitably activate the corrinoid substrate. One possible strategy for activating enzyme-bound Co^{2+}Cbl would involve replacing the axial DMB ligand (Figure 1) with a weaker donor to stabilize the redox-active Co d_{z^2}-based MO; for example, $DMB\rightarrow H_2O$ substitution is expected to raise E° by ~120 mV, corresponding to the difference in reduction potentials of Co^{2+}Cbl and $Co^{2+}Cbi^{+}$ ($E^{\circ} = -490$ mV).[17] However, the crystal structure of HOCbl bound to the CobA/ATP complex suggests that no such axial substitution actually occurs.[9] Likewise, our data conclusively demonstrate that when Co^{2+}Cbl binds to CobA, it retains the DMB lower axial ligand (Figures 4C and 6C). Nonetheless, while these observations rule out that CobA-bound Co^{2+}Cbl spontaneously converts to a typical "base-off" (i.e., $Co^{2+}Cbi^{+}$-like) species, our MCD and EPR data reveal that a small fraction is converted to a Co^{2+}corrinoid derivative with spectroscopic signatures reminiscent of square-planar Co^{2+} species (Table 1). Nearly complete conversion to this "activated" species is achieved when the physiologically more relevant substrate $Co^{2+}Cbi^{+}$ is used instead, presumably because the corresponding $Co-OH_2$ bond is weaker than the Co−DMB bond in Co^{2+}Cbl.[20] On the basis of our spectro/structural correlation, the lengthening of the lower ligand bond by ~0.3 Å, in the activated Co^{2+}corrinoid species (vide supra), results in a 0.266 eV stabilization of the Co $3d_{z^2}$-based redox-active MO. Such a change in electronic structure should raise the $Co^{2+/1+}$ reduction potential by ~250 mV, thereby ensuring ample thermodynamic driving force for the reduction of the CobA-bound Co^{2+}corrinoid substrate by FldA. The fact that this activated Co^{2+}corrinoid species is formed in high yield only in the presence of ATP provides a means by which the enzyme can control the timing of $Co^{2+}\rightarrow Co^{1+}$ reduction so as to protect itself from being attacked by the transiently formed Co^{1+}corrinoid "supernucleophile".

While we have demonstrated herein that CobA accomplishes the thermodynamically challenging $Co^{2+}\rightarrow Co^{1+}$corrinoid reduction step by promoting partial dissociation of the Co^{2+}corrinoid's lower axial ligand, a key question that remains is whether all Co−C bond-forming enzymes employ the same general strategy for $Co^{2+}\rightarrow Co^{1+}$corrinoid reduction despite their vastly different structures. Although answering this question is a major objective of ongoing research efforts in our laboratory, EPR and MCD spectroscopic data obtained for other members of this class of enzymes indeed hint toward a common mechanism for promoting reduction of the Co^{2+}corrinoid substrate.[66] By complementing spectroscopic studies with site-directed mutagenesis, we anticipate that significant new insight will be obtained into the detailed mechanism employed by these enzymes to achieve, and control the extent of, this extraordinary activation of their Co^{2+}-corrinoid substrates for one-electron reduction.

Acknowledgment. Financial support for this work was provided by the NSF (CAREER Grant MCB-0238530) and the Sloan Research Foundation Fellowship Program to T.C.B., and by the NIH (Grant GM40313) to J.C.E.-S. N.R.B. was supported by a Howard Hughes Medical Institute Fellowship, and funding for the EPR facilities was provided by the NSF (Grant CHE-093030). The authors thank Dr. Frank Neese (MPI Mülheim) for supplying free copies of the ORCA software package and the WEPR spectral fitting program, as well as his continued advice regarding DFT computations.

Supporting Information Available: Computational and experimental details, Cartesian coordinates for all computational models, predicted LF transition energies for "unperturbed" models and EPR parameters for selected models as a function of the $Co-OH_2$ bond length, Gaussian deconvolution parameters and fits for selected spectra, variable-temperature MCD spectra for all species studied, and WEPR input files for simulating EPR spectra (PDF). This material is available free of charge via the Internet at http://pubs.acs.org.

JA042142P

(65) Fonseca, M. V.; Escalante-Semerena, J. C. *J. Biol. Chem.* **2001**, *276*, 32101−32108.

(66) Stich, T. A.; Yamanishi, M.; Banerjee, R.; Brunold, T. C. *J. Am. Chem. Soc.* **2005**, *127*, 7660−7661.